Journal of Membrane Science 686 (2023) 121989

Contents lists available at ScienceDirect

Journal of Membrane Science

journal homepage: www.elsevier.com/locate/memsci

H_2S/CO_2 separation using sterically hindered amine membranes

Shraavya Rao [a], Yang Han [a], W.S. Winston Ho [a,b,*]

[a] William G. Lowrie Department of Chemical and Biomolecular Engineering, The Ohio State University, 151 West Woodruff Avenue, Columbus, OH, 43210-1350, USA
[b] Department of Materials Science and Engineering, The Ohio State University, 2041 College Road, Columbus, OH, 43210-1178, USA

ARTICLE INFO

Keywords:
Hydrogen sulfide
Carbon dioxide
Sterically hindered amine
Polymeric membrane

ABSTRACT

With the growing interest in carbon capture from syngas and natural gas, H_2S/CO_2 separation is gradually becoming important in the gas processing and carbon capture industries. This work describes the development of amine-based facilitated transport membranes (FTMs) suitable for syngas desulfurization. Six amino acid salt carriers with varying steric hindrance were synthesized and used to fabricate FTMs. Their H_2S/CO_2 separation performances were evaluated at 107 °C and 7 bar feed pressure, using a dry feed composition of 1.5% H_2S and 98.5% CO2. H_2S/CO_2 selectivity improved significantly as amine steric hindrance was increased. While mildly hindered amines showed low H_2S/CO_2 selectivities of around 5, sterically hindered and tertiary amines showed substantially improved separation performance, with selectivities in the range of 10–20. A highly hindered carrier containing the di-*tert*-butyl amine moiety showed the highest selectivity of 19.6, along with an H_2S permeance of 560 GPU. The di-*tert*-butyl amine-based FTM was used to study the effect of temperature and feed H_2S content on H_2S/CO_2 separation performance. The performances of the newly devised FTMs exceed the H_2S/CO_2 upper bound, and the learnings shed light on the design of amine carriers for acid gas separations.

1. Introduction

H_2S, an extremely toxic and corrosive gas, is a common contaminant in fuel gas mixtures such as syngas and natural gas. It poses significant risks to human health and can cause damage to equipment and pipelines [1,2]. To minimize occupational and safety hazards, desulfurization is an essential step in the processing of such gases. However, these fuel gases usually contain significant amounts of CO_2, which also needs to be removed prior to processing. For instance, syngas typically contains H_2 (55%), along with CO_2 (35–40%) and H_2S (0.1–3%) [3]. Similarly, natural gas also contains CO_2 (0–20%) and H_2S (0–5%) in addition to CH_4 (70–90%) [4]. Purification of such fuels generally involves the simultaneous removal of CO_2 and H_2S. At this stage, it is necessary to separate CO_2 and H_2S. This allows the safe sequestration of CO_2 and enables efficient sulfur recovery through the Claus process [5,6].

Both H_2S and CO_2 are acidic gases with similar kinetic sizes [7]. Due to their similar properties, CO_2 and H_2S can be difficult to separate through conventional desulfurization techniques [8,9]. Sub-ambient temperature processes, such as cryogenic distillation or Selexol physisorption, exploit the condensability differences between H_2S and CO_2 to separate them [10]. However, these methods incur significant cooling costs, which increases the overall energy requirement. Metal oxide sorbents such as ZnO or Fe_2O_3 can selectively desulfurize CO_2-containing gas streams at temperatures of 300–400 °C [11]. However, regeneration usually requires temperatures in excess of 600 °C, resulting in high energy consumption.

Amine absorption is the preferred method for acid gas separations [12,13]. Sterically hindered amine solvents can selectively desulfurize CO_2-containing gases [14–17]. However, absorption involves an energy-intensive and operationally complex regeneration step [18]. Moreover, corrosion and amine degradation are very common when dealing with highly acidic streams [18]. As a result, such systems require frequent maintenance and the use of expensive corrosion-resistant materials. An alternative approach that can mitigate corrosion is the use of solid amine-containing membranes in place of amine solvents. Such membranes, known as facilitated transport membranes (FTMs), can bypass the absorption-stripping cycle and offer advantages like improved energy-efficiency and operational simplicity [19].

Fig. 1 shows a schematic of an amine-based FTM and illustrates the reactive transport of acid gases across the membrane. The acid gases undergo a reversible reaction with the amine molecules or "carriers". The reaction products then diffuse across the membrane to release the

* Corresponding author. William G. Lowrie Department of Chemical and Biomolecular Engineering, The Ohio State University, 151 West Woodruff Avenue, Columbus, OH, 43210-1350, USA.
E-mail address: ho.192@osu.edu (W.S.W. Ho).

https://doi.org/10.1016/j.memsci.2023.121989
Received 11 June 2023; Received in revised form 29 July 2023; Accepted 8 August 2023
Available online 9 August 2023

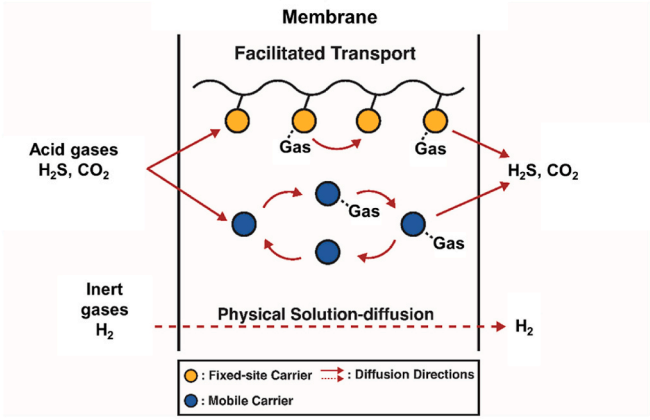

Fig. 1. Schematic of gas transport through an amine-based FTM. Adapted from Ref. 20 [20].

acid gas on the permeate side. Inert gases can only pass through the membrane via physical solution-diffusion. As a result, FTMs can exhibit very high permeability and selectivity for acid gases over inert gases.

FTMs have been extensively researched for CO_2/inert gas separations, and a number of publications have addressed the development of FTMs for post-combustion and pre-combustion carbon capture [20–27]. However, selectivity between two acid gases, such as H_2S and CO_2, has largely remained unexplored [28]. This work describes the synthesis of amine-containing FTMs specifically tailored to H_2S/CO_2 separation and investigates the effect of amine structure on H_2S/CO_2 separation performance.

Designing FTMs for H_2S/CO_2 separation requires an understanding of the mechanisms through which the amine-acid gas reactions proceed. Both H_2S and CO_2 are Lewis acids; however, their reactions with amines follow very different mechanisms. In the case of H_2S, the reaction follows a straightforward acid-base proton transfer mechanism [14]. Here, H_2S loses a proton to the amine, as shown in Equation (1).

$$H_2S + R_1R_2\text{–}NH \rightleftharpoons HS^- + R_1R_2\text{–}NH_2^+ \quad (1)$$

where R_1 represents an alkyl group and R_2 refers to an alkyl group or a hydrogen.

In contrast, the amine-CO_2 reaction is significantly more complicated. CO_2 does not contain acidic protons and cannot undergo proton transfer. Instead, the reaction can occur through two different routes: the carbamate pathway or the bicarbonate pathway [29,30].

In the carbamate pathway, predominantly observed for unhindered amines, the amine acts as a nucleophile and attacks the electropositive CO_2 carbon, forming a zwitterionic intermediate [13,31,32]. Equation (2) depicts the zwitterion formation reaction. In the subsequent step, the zwitterion is deprotonated by another amine to form a carbamate anion, as shown in Equation (3).

$$CO_2 + R_1R_2\text{–}NH \rightleftharpoons R_1R_2\text{–}NH^+\text{–}COO^- \quad (2)$$

$$R_1R_2\text{–}NH^+\text{–}COO^- + R_1R_2\text{–}NH \rightleftharpoons R_1R_2\text{–}N\text{–}COO^- + R_1R_2\text{–}NH_2^+ \quad (3)$$

The carbamate pathway is very sensitive to steric effects. The presence of bulky, sterically hindered substituents on the amine group impedes the nucleophilic attack of CO_2 and renders the carbamate unstable. Instead, for hindered and tertiary amines, the reaction follows the slower bicarbonate pathway [29,30,33]. Here, water acts as a nucleophile in the presence of an amine molecule and attacks CO_2. The bicarbonate pathway, depicted in Equation (4), provides more efficient reaction stoichiometry, with an amine/CO_2 ratio of 1:1, compared to the 2:1 ratio for the carbamate reaction.

$$CO_2 + R_1R_2\text{–}NH + H_2O \rightleftharpoons HCO_3^- + R_1R_2\text{–}NH_2^+ \quad (4)$$

Due to the slow kinetics of the bicarbonate pathway, sterically hindered amines can display selectivity for H_2S over CO_2. Such effects have been reported in amine adsorbent systems, where hindered amine adsorbents can achieve highly selective H_2S/CO_2 separation [34–37].

This is in contrast to hindered amine FTMs, where studies have reported that increasing amine hindrance substantially improved CO_2 permeability [20,22,38,39]. The improvement was attributed to hindered amines reacting preferentially through the more effective bicarbonate pathway, which resulted in an increased CO_2 capacity. However, it should be noted that these studies involved polymeric amine carriers [20,22,38,39]. The inclusion of sterically hindered substituents may have led to increased free volume and disrupted hydrogen bonding within the polymer, potentially confounding the impact of reaction chemistry.

This study aims to clarify the relationship between amine hindrance and acid gas transport by systematically investigating the effect of amine structure on the H_2S/CO_2 separation performance in FTMs. To minimize confounding effects of free volume, this study focuses exclusively on small-molecule mobile amine carriers. A number of amino acid salt carriers with varying alkyl substitution were evaluated for their H_2S/CO_2 separation performance. FTMs were fabricated by incorporating these carriers into a crosslinked poly(vinyl alcohol) (PVA) matrix. ^{1}H nuclear magnetic resonance (NMR) and Fourier transform infrared (FTIR) spectroscopy were employed to characterize the newly developed carriers and FTMs. An initial screening study was conducted by assessing the H_2S/CO_2 separation performances at two different carrier loadings. Sterically hindered amines were found to possess improved H_2S/CO_2 selectivity. An optimal FTM was identified and used to explore the effect of temperature and feed H_2S content on membrane performances. This new FTM exhibited exceptional H_2S/CO_2 transport performance and surpassed the H_2S/CO_2 upper bound.

2. Experimental

2.1. Materials

PVA POVAL 100-88 (94%, 87–89% hydrolysis degree) was provided by Kuraray America. Glacial acetic acid, potassium hydroxide (KOH), glycine, sarcosine, *N-tert*-butylglycine hydrochloride, sodium hydroxide (NaOH), glutaraldehyde (50% in water), sodium chloride (NaCl), and deuterium oxide (99.9% atom D, containing 0.05% wt.% of the sodium salt of 3-(trimethylsilyl)propionic-2,2,3,3-d_4 acid (NaTMSP)) were purchased from Sigma Aldrich. *N,N*-Dimethylglycine was purchased from Alfa-Aesar. Acetonitrile (ACN), chloroform (CH_3Cl), ethyl bromoacetate ($BrCH_2COOC_2H_5$), and isopropylamine were purchased from VWR Chemicals. Methanol (MeOH), acetone, potassium carbonate (K_2CO_3), and ethanol were purchased from Fisher Scientific.

Purolite® A600OH strong base anion-exchange resin and Purolite® C100H acid cation-exchange resin were donated by Purolite Corporation. Nanoporous polysulfone with an average pore size of 10 nm and a porosity of about 7% was purchased from TriSep Corporation. The feed gases, CO_2 and H_2S, and the helium required for gas chromatography (GC) were purchased from Praxair Inc.

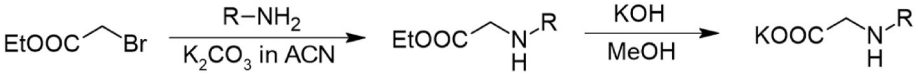

Fig. 2. Synthesis of *N*-isopropylglycine. R refers to the isopropyl group.

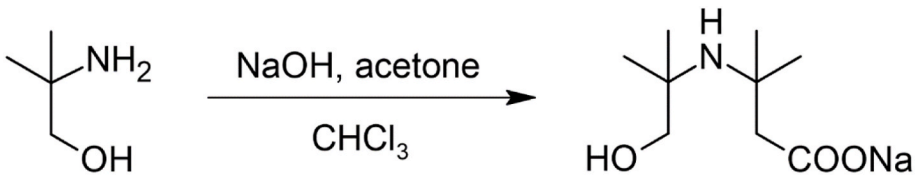

Fig. 3. Synthesis of *N*-(1,1-dimethyl-2-hydroxyethyl)-aminoisobutyric acid, via the Bargellini reaction.

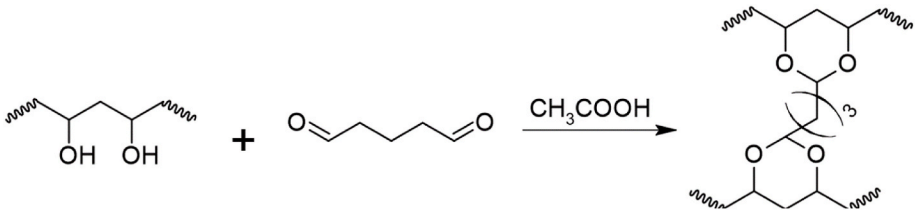

Fig. 4. Crosslinking of PVA.

2.2. Carrier synthesis

Glycine, sarcosine, and dimethylglycine were used as received without further purification. *N-tert*-butylglycine hydrochloride was dissolved in methanol to form a 5 wt% solution. The hydrochloride was removed through ion-exchange using Purolite® A600OH anion-exchange resin. Following the ion-exchange, the resin was filtered out. The methanol was evaporated out under vacuum to obtain the pure compound.

N-isopropylglycine was synthesized using ethyl bromoacetate and isopropylamine, as shown in Fig. 2. Ethyl bromoacetate (25 mmol) and isopropylamine (50 mmol) were added to 30 ml ACN. K_2CO_3 (50 mmol) was added dropwise as a 30 wt% solution in water. The reaction mixture was stirred overnight at room temperature. After the reaction, the solution was extracted with ethyl acetate and water. The organic phase was washed with 10% NaCl twice, and then evaporated under vacuum to obtain the crude ester. The ester was then dissolved in 20 ml of methanol along with 10 mmol KOH. The solution was stirred overnight at room temperature to complete the hydrolysis. KOH was removed using Purolite® C100H cation exchange resin. The solution was then evaporated under vacuum to obtain an off-white solid product. The product was washed with acetone and dried under vacuum to obtain *N*-isopropylglycine. The purity was confirmed to be >95% via ^{1}H NMR.

N-(1,1-dimethyl-2-hydroxyethyl)-aminoisobutyric acid was synthesized via the Bargellini reaction, shown in Fig. 3 [40]. The details of the reaction and mechanism, which have been covered elsewhere, are provided in Section S1 of the Supporting Information (SI) [41,42]. 2-Amino-2-methylpropan-1-ol (30 mmol), chloroform (15 mmol) and acetone (100 mmol) were added to a round bottom flask under stirring with the temperature controlled at 0 °C with an ethanol-water ice bath. Powdered NaOH (50 mmol) was added to the solution under nitrogen in 5 portions while keeping the temperature below 5 °C. The solution was stirred under nitrogen and allowed to reach room temperature overnight. The slurry obtained was filtered under vacuum and the filtrate collected. The solid residue was once again filtered with 100 ml of methanol. The combined filtrate was subjected to ion-exchange using Purolite® C100H to remove NaOH. The solution was then evaporated under vacuum to obtain an off-white solid residue. The solid residue was washed with acetone. The product thus obtained contained some inorganic impurities, which were removed by once again dissolving the solid in ethanol. The insoluble impurity was filtered off and the soluble *N*-(1,1-dimethyl-2-hydroxyethyl)-aminoisobutyric acid product was obtained by evaporating the ethanol under vacuum. The purity was confirmed to be >95% using ^{1}H NMR.

NMR samples were prepared by dissolving the product in D_2O to form a 1 wt% solution. The D_2O contained 0.05 wt% NaTMSP, which was used as a standard.

2.3. Crosslinking of PVA

PVA POVAL 100-88 (1 equivalent) was dissolved in water overnight to obtain a 4 wt% solution. In the synthesis of crosslinked PVA, glutaraldehyde (0.25 equivalent) was added to the solution as a crosslinker. A drop of glacial acetic acid was added to catalyze the crosslinking. The reaction is described in Fig. 4. The crosslinking reaction was carried out overnight at 35 °C. A significant increase in the viscosity was observed after crosslinking. The acetic acid was removed using Purolite® A600OH strong base anion-exchange resin.

2.4. Membrane preparation

A 5 wt% carrier solution was prepared by dissolving the amino acid carrier in water. A stoichiometric amount of KOH was added under stirring to deprotonate the amino acid and convert it to its amino acid salt carrier. The coating solution was prepared by adding the carrier solution dropwise to 4 wt% crosslinked PVA under vigorous stirring. After centrifuging at 3000 rpm for 5 min, the solution was coated on to a nanoporous polysulfone support with a GARDCO adjustable micrometer film applicator (Paul N. Gardner Company). The membrane was dried in a fume hood for half an hour and then cured at 120 °C for 6 h to complete the crosslinking. The thickness was measured using a Mitutoyo electronic indicator (Model 543-252B, Mitutoyo America Corp., Aurora, IL) with an accuracy of ±1 μm. Unless otherwise specified, the selective layer thickness was controlled at ca. 3 μm.

For FTIR characterization, freestanding films with a thickness of ca. 50 μm were prepared by coating the solution onto a glass plate. The films were dried in a fume hood and then cured at 120 °C for 6 h.

Water uptake measurements were conducted at 60 °C and 100% RH as per the procedure detailed in Ref. [43]. In the measurements, freestanding films were used.

2.5. Material characterization

In order to confirm incorporation of the carrier, the membrane samples were analyzed using attenuated total reflection (ATR) FTIR spectroscopy using a Nexus 470 Fourier transform infrared spectrometer (Nicolet Instruments Co., Waltham, MA). 32 scans were collected and averaged for each spectrum. The cross-sectional thickness was confirmed using Scanning Electron Microscopy (SEM, FEI Apreo LoVac, Thermo Fisher Scientific Inc., Waltham, MA). Carrier purities were confirmed using ^{1}H NMR. All NMR experiments were conducted using a Bruker Avance III 400 instrument.

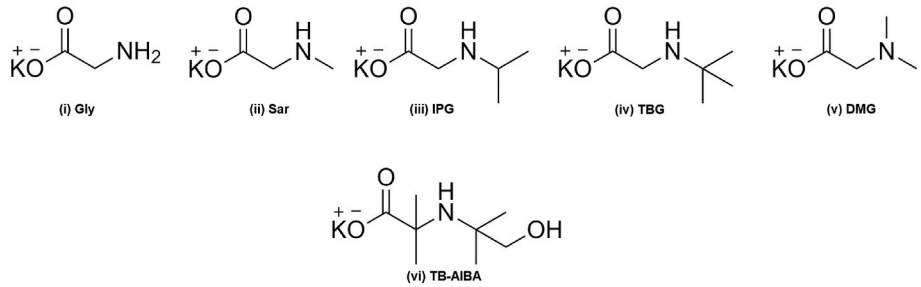

Fig. 5. Chemical structures of alt carriers used in this work. (i) Glycinate (Gly), (ii) Sarcosinate (Sar), (iii) *N*-isopropylglycinate (IPG), (iv) *N*-*tert*-butylglycinate (TBG), (v) *N,N*-dimethylglycinate (DMG), (vi) *N*-hydroxy-*tert*-butyl aminoisobutyrate (TB-AIBA).

A Wicke-Kallenbach permeation apparatus was used to measure the membrane transport properties. A detailed description of the setup can be found in a previous publication [27]. For convenience, a brief summary is provided here. The membrane was placed in a gas permeation cell with an area of 2.7 cm^2 for testing. The feed and sweep gases passed through stainless steel packed column humidifiers, before entering the permeation cell. The feed side was maintained at 100% relative humidity (RH), while the sweep water content was controlled at 85%, based on recommendations from prior publications [44,45]. After exiting the permeation cell, the gases passed through stainless steel water knockouts before entering the gas chromatograph (GC). The GC (Model 6890 N, Agilent Technologies), equipped with a micropacked column (80/100 Hayesep-D, Sigma-Aldrich) and a thermal conductivity detector (TCD), was used to analyze the concentrations of CO_2 and H_2S.

The membranes were tested at 107 °C and 7 bar feed pressure. For the initial carrier screening tests, a dry feed gas composition of 98.5% CO_2 and 1.5% H_2S was used before humidification. For investigating the dependence of H_2S permeance on feed H_2S content, the feed H_2S content was varied between 0.5 and 30%, with the balance being CO_2. The gas permeances and selectivity were calculated using Equations (5) – (7):

$$P_{H_2S} = J_{H_2S} \Big/ \frac{\Delta p_{feed,H_2S} - \Delta p_{ret,H_2S}}{ln\left(\Delta p_{feed,H_2S} \Big/ \Delta p_{ret,H_2S}\right)} \tag{5}$$

$$P_{CO_2} = J_{CO_2} \Big/ \frac{\Delta p_{feed,CO_2} - \Delta p_{ret,CO_2}}{ln\left(\Delta p_{feed,CO_2} \Big/ \Delta p_{ret,CO_2}\right)} \tag{6}$$

$$\alpha = \frac{P_{H_2S}}{P_{CO_2}} \tag{7}$$

where P_{H_2S} and P_{CO_2} denote the H_2S and CO_2 permeances, respectively, J_{H_2S} and J_{CO_2} the H_2S and CO_2 fluxes, respectively, and $\Delta p_{feed,i}$ and $\Delta p_{ret,i}$ the transmembrane partial pressure differentials at the feed inlet and retentate outlet for gas *i*, respectively. The uncertainty in the H_2S permeance was calculated to be ~8% based on an error propagation analysis [46].

3. Results and discussion

3.1. Carrier structures

A series of amino acid salt carriers with varying degrees of nucleophilicity was devised. Starting from the common glycinate, the steric hindrance on the nitrogen atom was steadily increased by varying the alkyl substituent and the degree of amine steric hindrance. Fig. 5 presents the structures of these carriers. Glycinate (Gly) is a primary amine. Sarcosinate, *N*-isopropylglycinate, *N*-*tert*-butylglycinate, and *N*-(1,1-dimethyl-2-hydroxyethyl)-aminoisobutyrate are secondary amines with increasing degree of amine steric hindrance. *N,N*-dimethylglycine is a tertiary amine.

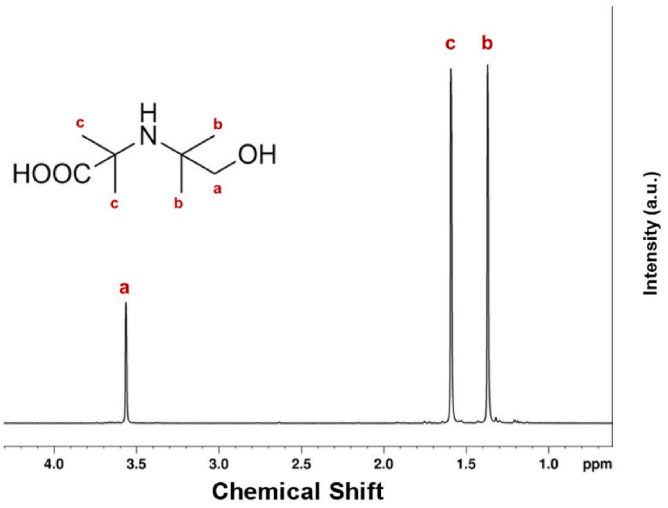

Fig. 6. ^1H NMR spectrum of *N*-hydroxy-*tert*-butyl aminoisobutyric acid.

It is worth mentioning that the anomalous structure of TB-AIBA was devised in order to mitigate solubility issues caused by the bulky *tert*-butyl groups. An analogous structure without a hydroxyl group was synthesized in the course of this work. However, it possessed poor water solubility and was incompatible with the PVA matrix.

3.2. Material characterization

This section describes the synthesis of the amine carriers and their incorporation into an FTM using the example of TB-AIBA. *N*-hydroxy-*tert*-butyl aminoisobutyric acid was synthesized from 2-amino-2-methyl-1-propanol, chloroform, and acetone via the Bargellini reaction, per a literature method [40]. Fig. 3 depicts the reaction scheme for the synthesis. After the synthesis, ^1H NMR was used to confirm the structure and purity of the product, which was >95% purity as mentioned earlier. Fig. 6 shows the proton NMR spectrum of *N*-hydroxy-*tert*-butyl aminoisobutyric acid.

Afterwards, the potassium salt of *N*-hydroxy-*tert*-butyl aminoisobutyric acid was synthesized and blended into crosslinked PVA. The solution was then cast into free-standing membranes. The FTIR spectra of crosslinked PVA and crosslinked PVA/TB-AIBA blend membranes (Fig. 7 (a)) confirmed the incorporation of the carrier into the PVA matrix. The blend spectrum showed distinctive peaks in the region over 3000 cm^{-1}, corresponding to the amino acid. The peak at 3000 cm^{-1} can be assigned to the N—H stretch of the secondary amine. The peak at 3300 cm^{-1} is attributed to the O—H stretch, with the broad band being a characteristic feature of hydrogen bonding. The broad peaks in the 3100–3500 cm^{-1} regions are intensified, indicating the presence of hydrogen bonding interactions between the PVA and the amino acid salt carriers in the blend membrane. Fig. 7 (b) shows the Scanning Electron

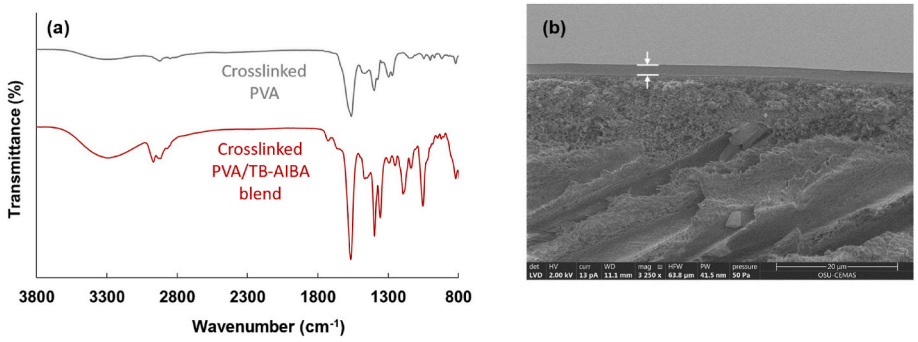

Fig. 7. (a) FTIR spectra of crosslinked PVA and TB-AIBA incorporated into crosslinked PVA. (b) SEM image of the cross-section of the thin-film composite membrane. The FTIR spectra of the remaining carriers incorporated into the crosslinked PVA have been provided in Section S2 of the SI.

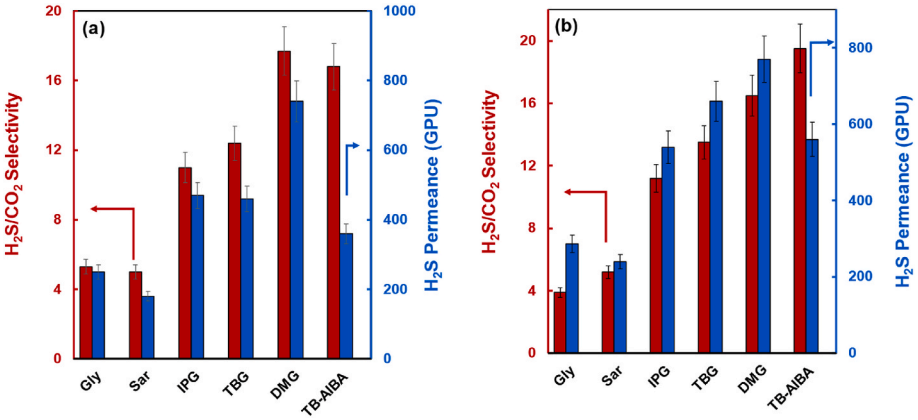

Fig. 8. H_2S permeances and H_2S/CO_2 selectivities for (a) 60 wt% carrier loading and (b) 70 wt% carrier loading. (GPU: gas permeation unit, 1 GPU=10^{-6} cm^3(STP) cm^{-2} s^{-1} $cmHg^{-1}$). Membranes were tested at 107 °C and 7 bar feed pressure. The feed relative humidity (RH) was 100% whereas the sweep water content was controlled to 85%. The dry feed gas composition was 1.5% H_2S with the balance being CO_2. The corresponding CO_2 permeances are available in Section S3 of the SI.

Microscopy (SEM) image of the cross-section of the composite membrane, in which a distinct selective layer of ca. 3 μm is visible.

3.3. *Effect of amine structure on H_2S/CO_2 separation performance*

Fig. 8 (a) and (b) present the H_2S/CO_2 transport performances of membranes incorporating 60 wt% and 70 wt% of carriers, respectively. As depicted in Fig. 8 (a), the sterically hindered amine carriers showed substantial improvements in H_2S/CO_2 selectivity and H_2S permeance compared to the less hindered amine carriers, i.e., more nucleophilic carriers. Gly and Sar showed poor H_2S/CO_2 selectivities of ca. 5. By contrast, the more hindered carriers, i.e., IPG, TBG, and TB-AIBA, showed over two-fold improvements in selectivity, with H_2S/CO_2 selectivities of 11, 12.4 and 16.8, respectively. The tertiary amine DMG showed a selectivity of 17.7.

Similar enhancements were observed in the H_2S permeances of the sterically hindered amines. Gly and Sar showed low H_2S permeances, of 250 and 180 GPU, respectively. IPG, TBG, and TB-AIBA showed higher H2S permeances, of 470, 460, and 360 GPU, respectively. DMG exhibited a high H_2S permeance of 740 GPU.

The same trend was observed at a higher carrier loading of 70 wt%. Hindered amines showed superior H_2S/CO_2 separation in comparison to unhindered and mildly hindered amines. Gly and Sar exhibited poor H_2S/CO_2 selectivity around 4–5. IPG, TBG, and TB-AIBA showed higher selectivities, of 11.2, 13.5, and 19.6, respectively. The H_2S/CO_2 selectivities have been plotted against the pKa_2 values of the amino acid carriers in Section S3 of the SI [47]; no clear trend is seen. This suggests that amine hindrance was the critical parameter investigated in this work. A more thorough investigation of the effect of amine hindrance on separation performance will be conducted in a future publication.

Interestingly, for the tertiary amine DMG, the H_2S/CO_2 selectivity decreased from 17.7 to 16.5 upon increasing the carrier content from 60 wt% to 70 wt%. At the higher carrier loading, the CO_2 permeance increased appreciably, whereas the rise in H_2S permeance was not quite as pronounced. This suggests that DMG may not be completely inert to CO_2. Accordingly, a mild increase in CO_2 facilitation occurred upon increasing the DMG content, causing the selectivity to drop.

At both carrier loadings, a marked enhancement in selectivity was observed as the amine steric hindrance increased from Sar to IPG. A similar increase was observed in the H_2S permeance. The rise in the separation performance of IPG could indicate that the shift from the carbamate pathway to the bicarbonate pathway occurs at this point. For IPG and the more hindered carriers, the amine-CO_2 reaction likely proceeds more through the bicarbonate pathway (slower kinetics) than the carbamate pathway (faster kinetics), leading to improved H_2S transport.

It should be noted that the H_2S/CO_2 selectivity of the neat crosslinked PVA membrane would not exceed 4. This was suggested from the pure-gas H_2S/CO_2 selectivity of the TB-AIBA-based FTM of 3.7, i.e., under complete carrier saturation, which represents the upper performance limit for membranes based on the solution-diffusion mechanism. The permeance of the neat crosslinked PVA membrane is too low to be measured experimentally, presumably due to the low water sorption of the neat crosslinked PVA under the conditions of this study.

Water uptake is known to play a role in enhancing acid gas permeance in FTMs [33]. In order to check if the H_2S/CO_2 separation performance was affected by the carriers' water sorption, water uptake measurements were conducted for freestanding films containing 70 wt%

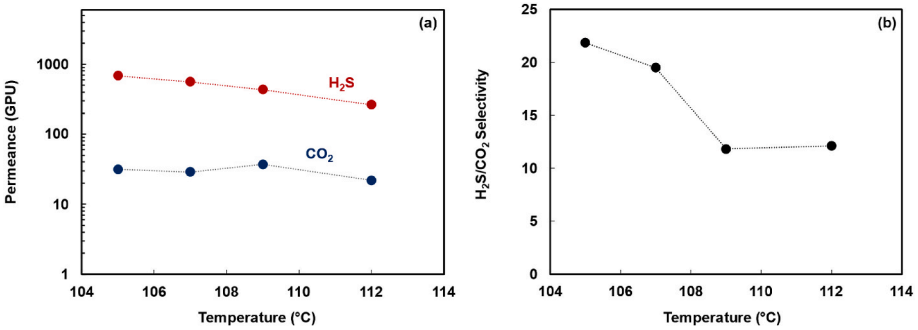

Fig. 9. (a) Variation of H_2S and CO_2 permeances and (b) variation of H_2S/CO_2 selectivity with temperature for FTM containing 70 wt% TB-AIBA. Membranes were tested at 7 bar feed pressure using a dry feed composition of 1.5% H_2S in CO_2. The feed RH was 100% whereas the sweep water content was controlled to 85%. The dotted lines are provided to guide the eyes and do not represent a fitting.

Gly in PVA, the least selective FTM, and 70 wt% TB-AIBA in PVA, the most selective FTM. A water uptake value of 180 ± 55% was measured for the FTM with Gly, while a water uptake value of 200 ± 75% was determined for the FTM with TB-AIBA. Given the similar uptake values, it was concluded that the carriers' structures do not affect water uptake significantly. Accordingly, the improvements in H_2S/CO_2 separation performance can be attributed entirely to the carriers' reactivities with H_2S and CO_2.

The FTM containing 70 wt% TB-AIBA was the most selective membrane, with an H_2S/CO_2 selectivity of 19.6, and an H_2S permeance of around 560 GPU. Upon further increasing the TB-AIBA content to 80 wt %, the H_2S permeance rose to 680 GPU. The H_2S/CO_2 selectivity also increased slightly, from 19.5 to 20. However, at the higher carrier loading, the membrane was prone to cracks and leaks during handling. This was likely due to the high loading of the crystalline carrier, which led to brittleness within the membrane. In order to avoid such issues, the membrane containing 70 wt% TB-AIBA was selected for further studies. This FTM was used to investigate the effect of temperature and feed H_2S partial pressure on H_2S transport.

3.4. Effect of temperature on H_2S/CO_2 separation performance

Fig. 9 presents the variation of H_2S/CO_2 separation performance with temperature, for the FTM containing 70 wt% of TB-AIBA. The effect of temperature was studied in the range 105–112 °C. The feed side was maintained at 100% RH, and the sweep side water content was fixed at 85%. As seen in Fig. 9 (a), temperature had a strong effect on the H_2S permeance. As the temperature rose from 105 to 112 °C, the H_2S permeance dropped two-fold from 685 GPU to 265 GPU. The CO_2 permeance varied non-monotonically, between 20 and 36 GPU. The H_2S/CO_2 selectivity dropped from 22 to ca. 12 over the same temperature range.

Such a drastic drop in permeance over the small temperature range is unusual. A slight decrease in permeability with temperature is expected — for example, for an FTM devised for CO_2/H_2 separation, the CO_2 permeance dropped by ca. 12% in the same temperature range [45]. This drop was attributed to a reduction in the FTM's water sorption capacity with increasing temperature, which hindered the diffusion of the reaction products across the membrane. While water retention likely plays a role in our system as well, reduced water sorption should affect CO_2 more severely than H_2S, since water is crucial to bicarbonate formation. The sharper decline in H_2S permeance suggests another effect might be at play. Studies of sterically hindered amines in absorption report that the selectivity for H_2S over CO_2 is kinetic [16]. Consequently, the selectivity for H_2S over CO_2 declines with temperature. The kinetics-derived selectivity for H_2S may compete with the effect of reduced water retention, giving rise to the trend obtained here. At 105–110 °C, the kinetic selectivity for H_2S over CO_2 decreases with increasing temperature. Over 110 °C, the reduced water sorption causes the CO_2 permeance to decline as well. As a result, the selectivity remained unchanged at ca. 12.

It should be mentioned that attempts to extend the range of temperatures proved unsuccessful. At 115 °C, the FTM showed very low permeance, possibly due to the reduced water content in the membrane at the higher temperature. Given the high content of crystalline carrier, low water sorption may have led to the formation of semicrystalline regions within the membrane, causing the permeability to crash. Similarly, at 102 °C, low permeance was observed, likely due to the slow reaction kinetics and low water content in the membrane at that temperature. Issues arising out of crystallinity can likely be remedied by the use of polymeric fixed site carriers such as sterically hindered polyamines. Such an approach will be explored in a future publication.

3.5. Effect of H_2S content in feed on H_2S/CO_2 separation performance

Finally, the performance of the TB-AIBA-containing FTM was

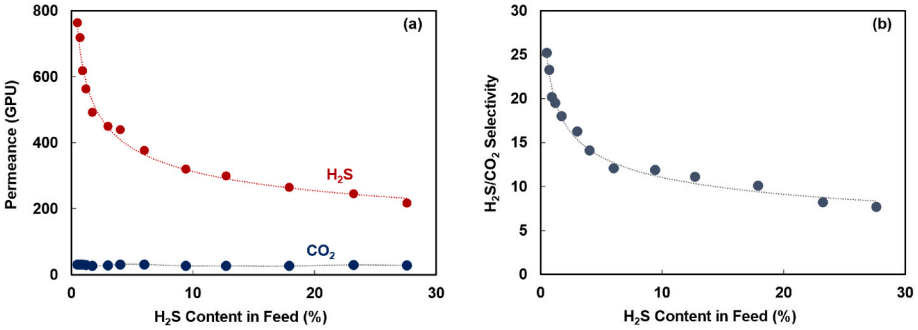

Fig. 10. Variation of (a) H_2S and CO_2 permeances and (b) H_2S/CO_2 selectivity as a function of feed H_2S content for the FTM containing 70 wt% TB-AIBA. Membranes were tested at 107 °C and 7 bar feed. The feed RH was 100% whereas the sweep water content was controlled to 85%. The dotted lines are provided to guide the eye and do not represent a fitting.

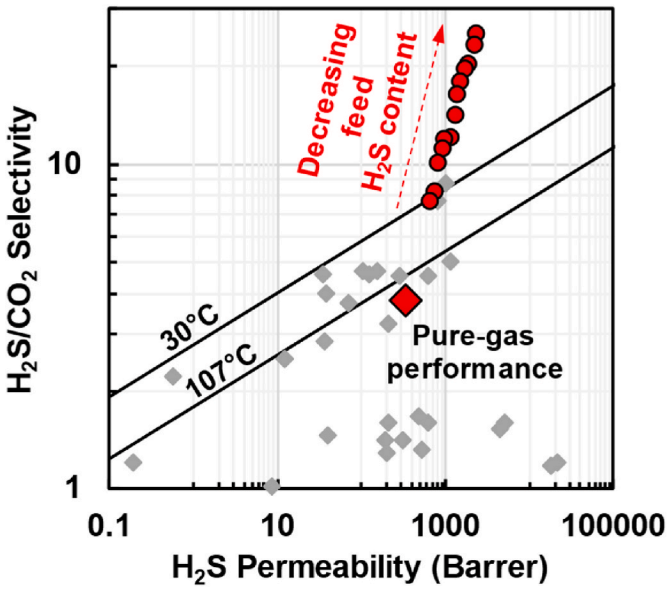

Fig. 11. Performance of FTM containing 70 wt% TB-AIBA against the H_2S/CO_2 upper bound. The pure-gas upper bounds have been calculated using the equation $\alpha_{H_2S/CO_2} = \beta_{oH_2S/CO_2} e^{\gamma/T} P_i^{-\lambda_{H_2S/CO_2}}$ [52]. The upper bound parameters λ_{H_2S/CO_2}, γ and β_{oH_2S/CO_2} take the values −0.1597, 659 K and 0.317 Barrer$^{-0.1597}$, respectively. The grey markers represent data reported by Scholes et al. and Harrigan et al. [49–51].

investigated under different H_2S contents. The overall feed pressure was kept constant at 7 bar, and the H_2S content was varied from 0.5 to 30%, with the balance gas being CO_2. Fig. 10 shows the effect of feed composition on H_2S/CO_2 separation performance at 107 °C.

As shown in Fig. 10 (a), the H_2S permeance exhibited a strong dependence on the H_2S partial pressure. As the feed H_2S content was increased, the H_2S permeance initially showed a steep drop, from 800 GPU at 0.5% H_2S to 400 GPU at 5% H_2S. This was followed by a more gradual decline, to 220 GPU at 27%. A similar trend was seen in the H_2S/CO_2 selectivity. At an H_2S content of 0.5%, the FTM showed a high selectivity of ca. 25. Upon increasing the H_2S content to 27%, the selectivity decreased to ca. 8.

Such a variation is characteristic of carrier saturation, a phenomenon which occurs due to the decrease in the concentration of free amine carriers at high acid gas partial pressures [48]. As the H_2S partial pressure is increased, an increasing number of carriers are taken up by the reaction with H_2S. As a result, the concentration of free carriers drops, causing a corresponding decrease in the H_2S permeance.

Interestingly, no such carrier saturation effect was observed for CO_2. The CO_2 permeance remained constant at ca. 30 GPU irrespective of the feed composition. This suggests that CO_2 passed through the FTM via solution-diffusion, rather than through facilitated transport. The high degree of hindrance effectively suppressed the CO_2-amine reaction, which freed up the carrier to facilitate H_2S transport and allowed the typical carrier saturation curve.

The phenomenon of carrier saturation enables an interesting feature of FTMs. For FTMs, the mixed-gas separation performance is always far superior to the pure-gas performance. The opposite is more commonly observed for conventional polymers, wherein plasticization and competitive sorption can negatively impact mixed-gas performance [48]. When tested under pure H_2S and pure CO_2, the TB-AIBA-containing FTM showed H_2S and CO_2 pure-gas permeances of 113 and 30 GPU, respectively. This corresponded to an 'ideal' pure-gas H_2S/CO_2 selectivity of 3.7. The selectivity and permeance obtained under mixed-gas conditions were markedly higher, highlighting the necessity of evaluating FTM performance at a range of feed compositions.

Despite the reduction in performance at high H_2S partial pressures, the TB-AIBA-containing FTM compares favorably with other membranes reported in literature [49–51]. Fig. 11 plots the performance of the newly developed FTM against the H_2S/CO_2 upper bounds. The pure-gas performance lies close to the 107 °C upper bound. The mixed-gas separation performance is significantly higher, outperforming both the 30 °C and the 107 °C upper bounds.

It should be mentioned that H_2S/CO_2 separation performance will decrease with increasing feed pressure. This is due to carrier saturation and competitive CO_2 reaction at higher acid gas partial pressures.

4. Conclusions

The use of sterically hindered amino acid salt carriers resulted in substantial improvements in H_2S/CO_2 separation performance. An FTM incorporating 70 wt% of a severely hindered amino acid salt carrier, TB-AIBA, showed the highest H_2S/CO_2 selectivity of 19.6 and an H_2S permeance of 560 GPU. The effects of temperature and feed H2S content on the performance of the TB-AIBA-containing membrane were investigated. Increasing temperature above 110 °C had a detrimental effect on H_2S/CO_2 separation performance. The optimal temperature was identified as 105 °C. Furthermore, increasing the feed H_2S content led to a drop in the H_2S permeance and H_2S/CO_2 selectivity due to carrier saturation. At H_2S contents of 0.5–27%, the FTM showed H_2S permeances of 765–220 GPU and H_2S/CO_2 selectivity of 25–8. Despite the reduction in performance at high H_2S contents, the separation performances of the TB-AIBA-containing FTM outperform the H_2S/CO_2 upper bounds, suggesting good potential for H_2S/CO_2 separation.

Declaration of Generative AI

ChatGPT was used in the preparation of this work to refine writing and improve readability. The authors have reviewed and edited the AI-generated content as necessary and take full responsibility for the contents of this publication.

Declaration of competing interest

The authors declare that they have no known competing financial interests or personal relationships that could have appeared to influence the work reported in this paper.

Data availability

Data will be made available on request.

Acknowledgements

We would like to thank Katharina Daniels, José D. Figueroa, and David Lang of the U.S. Department of Energy - National Energy Technology Laboratory (DOE-NETL) for their invaluable inputs and helpful discussions for this work. We gratefully acknowledge the funding from DOE-NETL under grant DE-FE0031635 and the Ohio Department of Development under grant OER-CDO-D-19-13. This work was partly supported by the Department of Energy under Award Number DE-FE0031635 with substantial involvement of the National Energy Technology Laboratory, Pittsburgh, PA, USA.

Appendix A. Supplementary data

Supplementary data to this article can be found online at https://doi.org/10.1016/j.memsci.2023.121989.

References

[1] B. Doujaiji, J.A. Al-Tawfiq, Hydrogen sulfide exposure in an adult male, Ann. Saudi Med. 30 (2010) 76–80, https://doi.org/10.4103/0256-4947.59379.

[2] M. Yadav, M.H. Sliem, A.M. Abdullah, K.M. Youssef, N.H. Al-Qahtani, Impact of prolonged exposure to sour service on the mechanical properties and corrosion mechanism of NACE carbon steel material used in wet sour gas multiphase pipeline, Sustainability 14 (2022) 8015, https://doi.org/10.3390/su14138015.

[3] K. Ramasubramanian, Y. Zhao, W.S. Winston Ho, CO_2 capture and H_2 purification: prospects for CO_2-selective membrane processes, AIChE J 59 (2013) 1033–1045, https://doi.org/10.1002/aic.14078.

[4] A. Fayazi, M. Arabloo, A.H. Mohammadi, Efficient estimation of natural gas compressibility factor using a rigorous method, J. Nat. Gas Sci. Eng. 16 (2014) 8–17, https://doi.org/10.1016/j.jngse.2013.10.004.

[5] L. Zheng, N. Spycher, J. Birkholzer, T. Xu, J. Apps, Y. Kharaka, On modeling the potential impacts of CO_2 sequestration on shallow groundwater: transport of organics and co-injected H_2S by supercritical CO_2 to shallow aquifers, Int. J. Greenh. Gas Control 14 (2013) 113–127, https://doi.org/10.1016/j.ijggc.2013.01.014.

[6] P.D. Clark, N.I. Dowling, M. Huang, W.Y. Svrcek, W.D. Monnery, Mechanisms of CO and COS formation in the Claus furnace, Ind. Eng. Chem. Res. 40 (2001) 497–508, https://doi.org/10.1021/ie990871l.

[7] A. Hayek, Y.A. Shalabi, A. Alsamah, Sour mixed-gas upper bounds of glassy polymeric membranes, Sep. Purif. Technol. 277 (2021), 119535, https://doi.org/10.1016/j.seppur.2021.119535.

[8] M.M. Tomadakis, H.H. Heck, M.E. Jubran, K. Al-Harthi, Pressure swing adsorption separation of H_2S from CO_2 with molecular sieves 4A, 5A, and 13X, Separ. Sci. Technol. 46 (2011) 428–433, https://doi.org/10.1080/01496395.2010.520292.

[9] H.H. Heck, M.L. Hall, R. Dos Santos, M.M. Tomadakis, Pressure swing adsorption separation of $H_2S/CO_2/CH_4$ gas mixtures with molecular sieves 4A, 5A, and 13X, Separ. Sci. Technol. 53 (2018) 1490–1497, https://doi.org/10.1080/01496395.2017.1417315.

[10] M.S. Shah, M. Tsapatsis, J.I. Siepmann, Hydrogen sulfide capture: from absorption in polar liquids to oxide, zeolite, and metal–organic framework adsorbents and membranes, Chem. Rev. 117 (2017) 9755–9803, https://doi.org/10.1021/acs.chemrev.7b00095.

[11] P.R. Westmoreland, D.P. Harrison, Evaluation of candidate solids for high-temperature desulfurization of low-Btu gases, Environ. Sci. Technol. 10 (1976) 659–661, https://doi.org/10.1021/es60118a010.

[12] A.K. Chakraborty, G. Astarita, K.B. Bischoff, CO_2 absorption in aqueous solutions of hindered amines, Chem. Eng. Sci. 41 (1986) 997–1003, https://doi.org/10.1016/0009-2509(86)87185-8.

[13] P.V. Danckwerts, The reaction of CO_2 with ethanolamines, Chem. Eng. Sci. 34 (1979) 443–446, https://doi.org/10.1016/0009-2509(79)85087-3.

[14] G. Sartori, W.S.W. Ho, D.W. Savage, G.R. Chludzinski, S. Wlechert, Sterically-hindered amines for acid-gas absorption, Separ. Purif. Methods 16 (1987) 171–200, https://doi.org/10.1080/03602548708058543.

[15] A.K. Saha, S.S. Bandyopadhyay, P. Saju, A.K. Biswas, Selective removal of hydrogen sulfide from gases containing hydrogen sulfide and carbon dioxide by absorption into aqueous solutions of 2-amino-2-methyl-1-propanol, Ind. Eng. Chem. Res. 32 (1993) 3051–3055, https://doi.org/10.1021/ie00024a013.

[16] B.P. Mandal, A.K. Biswas, S.S. Bandyopadhyay, Selective absorption of H_2S from gas streams containing H_2S and CO_2 into aqueous solutions of *N*-methyldiethanolamine and 2-amino-2-methyl-1-propanol, Sep. Purif. Technol. 35 (2004) 191–202, https://doi.org/10.1016/S1383-5866(03)00139-4.

[17] J.-G. Lu, Y.-F. Zheng, D.-L. He, Selective absorption of H_2S from gas mixtures into aqueous solutions of blended amines of methyldiethanolamine and 2-tertiarybutylamino-2-ethoxyethanol in a packed column, Sep. Purif. Technol. 52 (2006) 209–217, https://doi.org/10.1016/j.seppur.2006.04.003.

[18] R.W. Baker, K. Lokhandwala, Natural gas processing with membranes: an overview, Ind. Eng. Chem. Res. 47 (2008) 2109–2121, https://doi.org/10.1021/ie071083w.

[19] T.C. Merkel, M. Zhou, R.W. Baker, Carbon dioxide capture with membranes at an IGCC power plant, J. Membr. Sci. 389 (2012) 441–450, https://doi.org/10.1016/j.memsci.2011.11.012.

[20] T.-Y. Chen, X. Deng, L.-C. Lin, W.S.W. Ho, New sterically hindered polyvinylamine-containing membranes for CO_2 capture from flue gas, J. Membr. Sci. 645 (2022), 120195, https://doi.org/10.1016/j.memsci.2021.120195.

[21] A. Hussain, M.-B. Hägg, A feasibility study of CO_2 capture from flue gas by a facilitated transport membrane, J. Membr. Sci. 359 (2010) 140–148, https://doi.org/10.1016/j.memsci.2009.11.035.

[22] Y. Zhao, W.S. Winston Ho, Steric hindrance effect on amine demonstrated in solid polymer membranes for CO_2 transport, J. Membr. Sci. (2012) 415–416, https://doi.org/10.1016/j.memsci.2012.04.044, 132–138.

[23] I. Taniguchi, S. Duan, T. Kai, S. Kazama, H. Jinnai, Effect of the phase-separated structure on CO_2 separation performance of the poly(amidoamine) dendrimer immobilized in a poly(ethylene glycol) network, J. Mater. Chem. A 1 (2013), 14514, https://doi.org/10.1039/c3ta13711b.

[24] I. Taniguchi, T. Kai, S. Duan, S. Kazama, H. Jinnai, A compatible crosslinker for enhancement of CO_2 capture of poly(amidoamine) dendrimer-containing polymeric membranes, J. Membr. Sci. 475 (2015) 175–183, https://doi.org/10.1016/j.memsci.2014.10.015.

[25] V. Vakharia, K. Ramasubramanian, W.S.W. Ho, An experimental and modeling study of CO_2-selective membranes for IGCC syngas purification, J. Membr. Sci. 488 (2015) 56–66, https://doi.org/10.1016/j.memsci.2015.04.007.

[26] S. Rafiq, L. Deng, Hägg, May-Britt, Role of facilitated transport membranes and composite membranes for efficient CO_2 capture - a review, ChemBioEng Rev. 3 (2016) 68–85, https://doi.org/10.1002/cben.201500013.

[27] K.K. Chen, W. Salim, Y. Han, M. Gasda, W.S.W. Ho, Fluoride- and hydroxide-containing CO_2-selective membranes for improving H_2 utilization of solid oxide fuel cells, J. Membr. Sci. 612 (2020), 118484, https://doi.org/10.1016/j.memsci.2020.118484.

[28] J.H. Meldon, A. Dutta, Analysis of ultimate permselectivity for H_2S over CO_2 in alkaline solutions, Chem. Eng. Sci. 49 (1994) 689–697, https://doi.org/10.1016/0009-2509(94)85015-1.

[29] T. Davran-Candan, DFT modeling of CO_2 interaction with various aqueous amine structures, J. Phys. Chem. A 118 (2014) 4582–4590, https://doi.org/10.1021/jp503929g.

[30] M. Narimani, S. Amjad-Iranagh, H. Modarress, CO_2 absorption into aqueous solutions of monoethanolamine, piperazine and their blends: quantum mechanics and molecular dynamics studies, J. Mol. Liq. 233 (2017) 173–183, https://doi.org/10.1016/j.molliq.2017.03.015.

[31] M. Caplow, Kinetics of carbamate formation and breakdown, J. Am. Chem. Soc. 90 (1968) 6795–6803, https://doi.org/10.1021/ja01026a041.

[32] P.M.M. Blauwhoff, G.F. Versteeg, W.P.M. Van Swaaij, A study on the reaction between CO_2 and alkanolamines in aqueous solutions, Chem. Eng. Sci. 38 (1983) 1411–1429, https://doi.org/10.1016/0009-2509(83)80077-3.

[33] X. Deng, C. Zou, Y. Han, L.-C. Lin, W.S.W. Ho, Computational evaluation of carriers in facilitated transport membranes for postcombustion carbon capture, J. Phys. Chem. C 124 (2020) 25322–25330, https://doi.org/10.1021/acs.jpcc.0c07627.

[34] J.J. Lee, C.-J. Yoo, C.-H. Chen, S.E. Hayes, C. Sievers, C.W. Jones, Silica-supported sterically hindered amines for CO_2 capture, Langmuir 34 (2018) 12279–12292, https://doi.org/10.1021/acs.langmuir.8b02472.

[35] C.N. Okonkwo, C. Okolie, A. Sujan, G. Zhu, C.W. Jones, Role of amine structure on hydrogen sulfide capture from dilute gas streams using solid adsorbents, Energy Fuel. 32 (2018) 6926–6933, https://doi.org/10.1021/acs.energyfuels.8b00936.

[36] C.N. Okonkwo, H. Fang, D.S. Sholl, J.E. Leisen, C.W. Jones, Effect of humidity on the sorption of H_2S from multicomponent acid gas streams on silica-supported sterically hindered and unhindered amines, ACS Sustain. Chem. Eng. 8 (2020) 10102–10114, https://doi.org/10.1021/acssuschemeng.0c02012.

[37] C.N. Okonkwo, J.J. Lee, A. De Vylder, Y. Chiang, J.W. Thybaut, C.W. Jones, Selective removal of hydrogen sulfide from simulated biogas streams using sterically hindered amine adsorbents, Chem. Eng. J. 379 (2020), 122349, https://doi.org/10.1016/j.cej.2019.122349.

[38] Y. Zhao, W.S.W. Ho, CO_2-selective membranes containing sterically hindered amines for CO_2/H_2 separation, Ind. Eng. Chem. Res. 52 (2013) 8774–8782, https://doi.org/10.1021/ie301397m.

[39] Z. Tong, W.S.W. Ho, New sterically hindered polyvinylamine membranes for CO_2 separation and capture, J. Membr. Sci. 543 (2017) 202–211, https://doi.org/10.1016/j.memsci.2017.08.057.

[40] K. Zhang, B.B. Noble, A.C. Mater, M.J. Monteiro, M.L. Coote, Z. Jia, Effect of heteroatom and functionality substitution on the oxidation potential of cyclic nitroxide radicals: role of electrostatics in electrochemistry, Phys. Chem. Chem. Phys. 20 (2018) 2606–2614, https://doi.org/10.1039/C7CP07444A.

[41] S.D. Rychnovsky, T. Beauchamp, R. Vaidyanathan, T. Kwan, Synthesis of chiral nitroxides and an unusual racemization reaction, J. Org. Chem. 63 (1998) 6363–6374, https://doi.org/10.1021/jo9808831.

[42] M. Serafini, I. Murgia, M. Giustiniano, T. Pirali, G.C. Tron, The 115 years old multicomponent Bargellini reaction: perspectives and new applications, Molecules 26 (2021) 558, https://doi.org/10.3390/molecules26030558.

[43] X. Deng, Y. Han, L.-C. Lin, W.S.W. Ho, Computational prediction of water sorption in facilitated transport membranes, J. Phys. Chem. C 126 (2022) 3661–3670, https://doi.org/10.1021/acs.jpcc.1c09259.

[44] R. Xing, W.S.W. Ho, Crosslinked polyvinylalcohol–polysiloxane/fumed silica mixed matrix membranes containing amines for CO_2/H_2 separation, J. Membr. Sci. 367 (2011) 91–102, https://doi.org/10.1016/j.memsci.2010.10.039.

[45] L. Ansaloni, Y. Zhao, B.T. Jung, K. Ramasubramanian, M.G. Baschetti, W.S.W. Ho, Facilitated transport membranes containing amino-functionalized multi-walled carbon nanotubes for high-pressure CO_2 separations, J. Membr. Sci. 490 (2015) 18–28, https://doi.org/10.1016/j.memsci.2015.03.097.

[46] P.R. Bevington, D.K. Robinson, J.M. Blair, A.J. Mallinckrodt, S. McKay, Data reduction and error analysis for the physical sciences, Comput. Phys. 7 (1993) 415–416.

[47] J. Szegezdi, F. Csizmadia, Method for calculating the pKa values of small and large molecules, in: Abstr. Pap. Am. Chem. Soc., American Chemical Society, 1155 16th St, NW, Washington DC 20036 USA, 2007. http://www.chemaxon.com/product/pka.html.

[48] N.E. León, Z. Liu, M. Irani, W.J. Koros, How to get the best gas separation membranes from state-of-the-art glassy polymers, Macromolecules 55 (2022) 1457–1473, https://doi.org/10.1021/acs.macromol.1c01758.

[49] C.A. Scholes, S.E. Kentish, G.W. Stevens, Effects of minor components in carbon dioxide capture using polymeric gas separation membranes, Separ. Purif. Rev. 38 (2009) 1–44, https://doi.org/10.1080/15422110802411442.

[50] D.J. Harrigan, J. Yang, B.J. Sundell, J.A. Lawrence, J.T. O'Brien, M.L. Ostraat, Sour gas transport in poly(ether-*b*-amide) membranes for natural gas separations,

J. Membr. Sci. 595 (2020), 117497, https://doi.org/10.1016/j.memsci.2019.117497.

[51] D.J. Harrigan, J.A. Lawrence, H.W. Reid, J.B. Rivers, J.T. O'Brien, S.A. Sharber, B. J. Sundell, Tunable sour gas separations: simultaneous H_2S and CO_2 removal from natural gas via crosslinked telechelic poly(ethylene glycol) membranes, J. Membr. Sci. 602 (2020), 117947, https://doi.org/10.1016/j.memsci.2020.117947.

[52] B.W. Rowe, L.M. Robeson, B.D. Freeman, D.R. Paul, Influence of temperature on the upper bound: theoretical considerations and comparison with experimental results, J. Membr. Sci. 360 (2010) 58–69, https://doi.org/10.1016/j.memsci.2010.04.047.